PAPER

Doping-dependent nucleation of basal plane dislocations in 4H-SiC

IOP Publishing Journal of Physics D: Applied Physics
J. Phys. D: Appl. Phys. **55** (2022) 334002 (7pp) https://doi.org/10.1088/1361-6463/ac7178

Doping-dependent nucleation of basal plane dislocations in 4H-SiC

Xiaoshuang Liu[1,2,3], Rong Wang[2,3,*], Junran Zhang[1,2,3], Yunhao Lu[1,2], Yiqiang Zhang[4], Deren Yang[2,3] and Xiaodong Pi[2,3,*]

[1] Zhejiang Province Key Laboratory of Quantum Technology and Device, Department of Physics, Zhejiang University, Hangzhou 310027, People's Republic of China
[2] State Key Laboratory of Silicon Materials & School of Materials Science and Engineering, Zhejiang University, Hangzhou, Zhejiang, 310027, People's Republic of China
[3] Institute of Advanced Semiconductors & Zhejiang Provincial Key Laboratory of Power Semiconductor Materials and Devices, Hangzhou Innovation Center, Zhejiang University, Hangzhou, Zhejiang, 311200, People's Republic of China
[4] School of Materials Science and Engineering and Henan Institute of Advanced Technology, Zhengzhou University, Zhengzhou, Henan 450001, People's Republic of China

E-mail: rong_wang@zju.edu.cn and xdpi@zju.edu.cn

Received 14 February 2022, revised 14 April 2022
Accepted for publication 19 May 2022
Published 7 June 2022

Abstract

Basal plane dislocations (BPDs) are one of the most harmful dislocations in 4H silicon carbide (4H-SiC). Understanding the nucleation of BPDs is the basis of reducing the density of BPDs in 4H-SiC. In this work, we investigate the nucleation mechanism of BPDs, as well as the effect of doping on the nucleation of BPDs in 4H-SiC using nanoindentation. It is found that the shear stress plays a dominant role in the nucleation of BPDs in undoped 4H-SiC. This indicates that the shear component of the thermal stress during the growth of 4H-SiC single crystals and that of the mechanical stress during the processing of 4H-SiC wafers both give rise to the nucleation of BPDs. Nitrogen (N) doping is found to facilitate the nucleation of BPDs and decrease the shear stress required for the nucleation of BPDs. In contrast, vanadium (V) doping hinders the nucleation of BPDs, which promotes the polymorph transition from 4H-SiC to 3C-SiC.

Keywords: 4H-SiC, dislocations, doping, mechanical properties

(Some figures may appear in color only in the online journal)

1. Introduction

Owing to the advantages of the wide bandgap, high breakdown electric field strength, and high thermal conductivity, 4H silicon carbide (4H-SiC) is leaping in an explosive growth in high-power and high-frequency electronics [1–3]. 4H-SiC single crystals are usually grown by the sublimation or solution growth technique, during which the thermal stress gives rise to the formation of dislocations [4]. It is believed that threading dislocations in 4H-SiC single crystals usually inherit from the seed crystals, while basal plane dislocations (BPDs) usually derive from the thermal stress during the single-crystal growth [5]. After the single crystal growth, a 4H-SiC boule is processed into wafers by slicing, lapping and chemical–mechanical polishing (CMP) [6]. Because of the high hardness and brittleness of 4H-SiC, the processing of 4H-SiC wafers encounters the challenges of high processing loss, low efficiency, and low yield [7]. Although the later processing step can remove surface damages created in the former step, high density of subsurface defects still remain in 4H-SiC wafers, as a result of the mechanical stress [8]. It has been found that BPDs dominate the defect configurations during the processing of 4H-SiC wafers [9]. Therefore, understanding the nucleation of BPDs is critical to the optimization of the processing of 4H-SiC wafers, while the nucleation of

* Authors to whom any correspondence should be addressed.

BPDs induced by the mechanical processing is rarely studied. Furthermore, nitrogen (N) doping and vanadium (V) doping are the most commonly used dopants to tailor the electronic properties of 4H-SiC [10, 11]. Understanding the effect of N and V on the nucleation of BPDs is of great importance to the growth optimization and processing design of differently doped 4H-SiC wafers.

Although it is difficult to establish *in situ* technologies to investigate the effect of thermal stress and mechanical stress on the nucleation of BPDs, researchers have found that nanoindentation is a powerful experimental approach to introduce stress and investigate the generation and evolution of defects under different stresses [12, 13]. The mechanical properties of materials, such as the elastic modulus and hardness, can be extracted from the load-displacement curve by using the Oliver–Pharr approach [14–16]. During the loading and unloading of mechanical stress, the behaviors of defects, such as the dislocation nucleation and phase transitions, can be detected by the pop-in or pop-out event in a high-resolution load-displacement curve [17, 18]. Combining other characterization technologies, the generation and evolution mechanism of structural defects can be clarified.

In this work, nanoindentation tests and transmission electron microscopy (TEM) are employed to investigate the nucleation of BPDs in 4H-SiC. It turns out that shear stress prevails over tensile stress in the low-load nanoindentation-induced stress field, which gives rise to the nucleation of BPDs in undoped 4H-SiC. We find that N doping facilitates the BPD nucleation and decreases the shear stress required for the nucleation of BPDs. In contrast, V doping hinders the nucleation of BPDs, which promotes the polymorph transition from 4H-SiC to 3C-SiC. Our work completes the understanding on the nucleation of BPDs in 4H-SiC, and paves the way for the growth optimization and processing design of differently doped 4H-SiC wafers by reducing the density of BPDs.

2. Samples and methods

Undoped, N-doped, and V-doped 4H-SiC wafers were purchased from SICC Co., Ltd. The thicknesses of undoped, N-doped, and V-doped 4H-SiC wafers are 500 μm, 350 μm, and 500 μm, respectively. The doping concentration of N and V in N-doped and V-doped 4H-SiC are in the order of 10^{19} and 10^{16} cm^{-3}, respectively. The silicon (Si)-face of the 4H-SiC wafers were treated by CMP, with the surface roughness being smaller than 0.2 nm. Nanoindentation tests were carried out using a nanoindentation system (Hysitron TI980, Bruker, USA) with a Berkovich indenter. Since the nucleation of BPDs usually occurs during the early-stage displacements under low loads, a series of nanoindentation tests were performed under various peak loads ranging from 1 to 5 mN, with loading/unloading time of 10 s and holding time of 5 s. Before each test, the system was calibrated using a standard fused-silica specimen. The loading/unloading cycles were repeated for eight times to obtain reliable data.

A focused ion beam (Helios 5 UX, FEI, USA) was employed to prepare the cross-sectional TEM specimens of the indents. The surface of the indent was firstly passivated by a 1 μm thick Pt strip for protection. Initial trenches were milled on both sides of the indent, the central 4H-SiC was cut from three sides. A lower beam current was then utilized to thin the 4H-SiC to lower than 100 nm. TEM and high resolution TEM (HRTEM) were carried out using the FEI Tecnai G^2 TEM operated with an accelerating voltage of 300 kV.

3. Results and discussion

Figure 1 shows the typical load-displacement (*P–h*) curves of 4H-SiC subjected to various loads. For undoped 4H-SiC subjected to the load of 2 mN, the displacement is completely recoverable during the loading–unloading cycle, indicating the elastic deformation of 4H-SiC under the low load (figure 1(a)). When the load increases to 3 mN, the displacement of 4H-SiC cannot be completely recovered. The pop-in event occurs at the penetration depth of 47 nm, which corresponds to the load of 2.6 mN (figure 1(b)). Therefore, the onset of the plasticity of undoped 4H-SiC occurs at the load of 2.6 mN. It should be noted that the positions of the first pop-in event do not change when the load increases up to 5 mN (figure 1(c)). This indicates that the displacement of the pop-in event is independent of the load. We then compare the effect of doping on the positions of the pop-in events for differently doped 4H-SiC under the load of 3 mN. As shown in figure 1(d), the pop-in events of N-doped and V-doped 4H-SiC occur at the penetration depths of 33 and 37 nm, respectively. This indicates that the load triggering the pop-in event of 4H-SiC increases in the order of N doping, V doping and undoping.

The pop-in events in *P–h* curves are usually associated to the structural changes, that is the generation or evolution of defects beneath the indenter. For 4H-SiC subjected to low loads, the pop-in event is usually attributed to the formation of BPDs, micro cracks and polymorph transitions [19]. When the shear stress under the indenter is larger than the theoretical shear stress of the indented sample, the elastic–plastic transition would induce the nucleation of BPDs. When the tensile stress under the indenter is larger than the theoretical cleavage stress of the indented sample, the micro cracks would form during the indentation [18, 20]. In order to explore the origin of the pop-in event, as well as the effect of doping on the initial plastic deformation mechanism, we calculate the stress underneath the indenter under various loads. As shown in figure 1(a), the *P–h* curve under the elastic deformation range can be fitted by $P = 7.5 \times h^{1.5}$. Under the low loads exerted in this work, it is believed that the indenter is spherical instead of Berkovich [13]. Therefore, the *P–h* curve can be fitted by the Hertzian elastic contact theory [21]:

$$P = \frac{4}{3} E_r \sqrt{R} h^{\frac{3}{2}} \tag{1}$$

where P is the nanoindentated load, h is the displacement of the indenter, R is the radius of indenter. E_r is the reduced elastic modulus, which is calculated by:

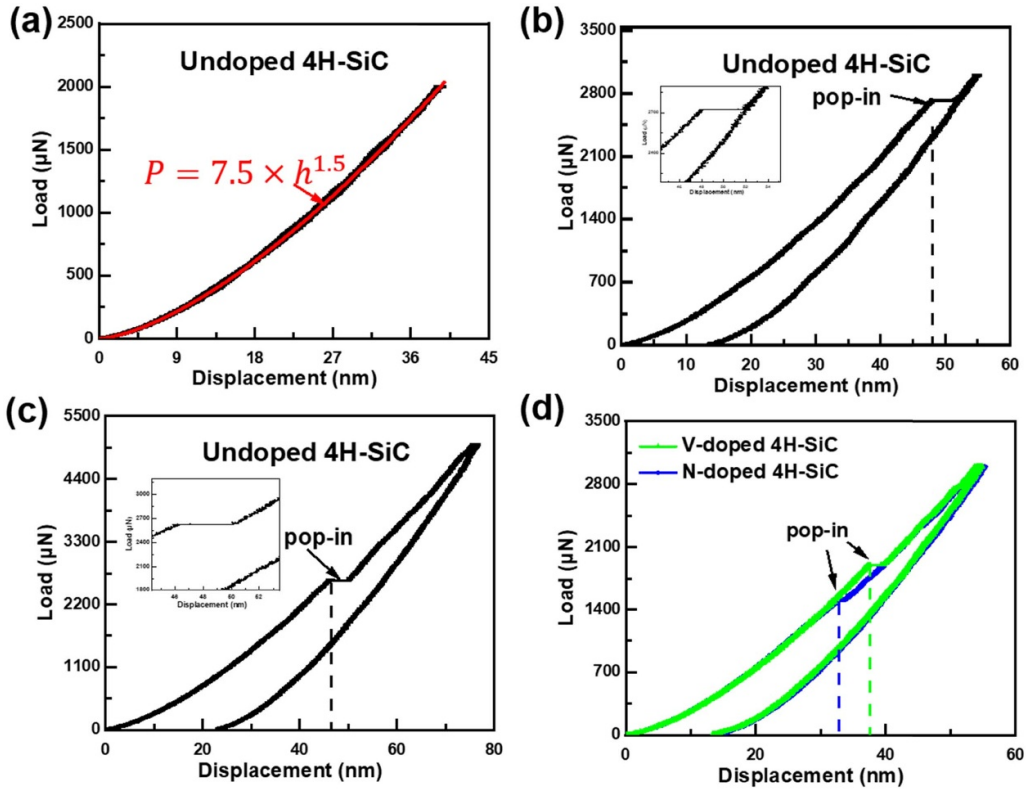

Figure 1. *P-h* curves for 4H-SiC under the loads of (a) 2 mN, (b) 3 mN and (c) 5 mN, with the pop-in events shown in the insets. (d) *P–h* curves for the N-doped and V-doped 4H-SiC under the load of 3 mN.

$$\frac{1}{1-E_{\mathrm{r}}}=\frac{1-\nu_{\mathrm{s}}^{2}}{1-E_{\mathrm{s}}}+\frac{1-\nu_{\mathrm{i}}^{2}}{1-E_{\mathrm{i}}} \tag{2}$$

where E_{s} (or E_{i}) and ν_{s} (or ν_{i}) are the elastic modulus and Poisson's ratios of 4H-SiC (or the diamond indenter), respectively [22]. With equations (1) and (2), the value of R is estimated to be 260 nm.

The shear stress (τ_{c}) beneath the indenter is then calculated by [23]:

$$\tau_{\mathrm{c}}=0.31\left(\frac{6PE_{\mathrm{r}}^{2}}{\pi^{3}R^{2}}\right)^{\frac{1}{3}} \tag{3}$$

The values of τ_{c} are compared to that of the theoretical shear strength (τ_{th}) of 4H-SiC, to evaluate whether the shear-stress induced dislocation nucleation happens during loading. The value of τ_{th} is calculated by [24]:

$$\tau_{\mathrm{th}}=\frac{G}{2\pi} \tag{4}$$

where G is the shear modulus of 4H-SiC, which can be determined by $G=\frac{E_{\mathrm{s}}}{2\times(1+\nu)}$. The values of elastic modulus obtained by the nanoindentation tests for undoped 4H-SiC, N-doped 4H-SiC and V-doped 4H-SiC are 455.19 ± 6.21 GPa, 394.14 ± 6.43 GPa and 486.42 ± 5.81 GPa, respectively. As shown in figure 2(a), during the nanoindentation of undoped 4H-SiC, the shear stress rapidly increases and reaches the theoretical shear stress (τ_{th}) at the pop-in depth. This indicates that the shear stress dominates the deformation stress field of the nanoindentated 4H-SiC, which gives rise to the nucleation of dislocations. The calculated stress of the nanoindentated N-doped 4H-SiC is similar to that of undoped 4H-SiC (figure 2(b)), indicating that N doping only reduces the shear stress required for the occurrence of the pop-in event, and does not change the dominant role of shear stress in the stress field of nanoindentated N-doped 4H-SiC. For V-doped 4H-SiC, the shear stress under the indenter is always less than the theoretical shear stress (figure 2(c)). This indicates that BPDs are less likely to be involved in the plasticity of V-doped 4H-SiC. In order to clearly analyze the shear stress of the pop-in event, the maximum shear stresses of the pop-in event are summarized in table 1. For undoped and N-doped 4H-SiC, the calculated shear stresses of the pop-in events are basically equal to the theoretical shear strength. This verifies that shear-stress induced dislocation nucleation gives rise to the pop-in event for nanoindentated undoped and N-doped 4H-SiC. For V-doped 4H-SiC, the calculated shear stresses during the whole loading–unloading cycle are always lower than the theoretical shear stress of 4H-SiC. This indicates that dislocation nucleation is not involved in the pop-in event of indented V-doped 4H-SiC.

The tensile stress and the theoretical cleavage strength (σ_{th}) of 4H-SiC are then compared to clarify whether micro cracks are formed during the pop-in event. The tensile stress (σ_{c}) under the indenter is calculated by [25]:

$$\sigma_{\mathrm{c}}=\left(\frac{1-2\upsilon}{2\pi}\right)\left(\frac{4E_{\mathrm{r}}}{3R}\right)^{\frac{1}{3}}P^{\frac{1}{3}}. \tag{5}$$

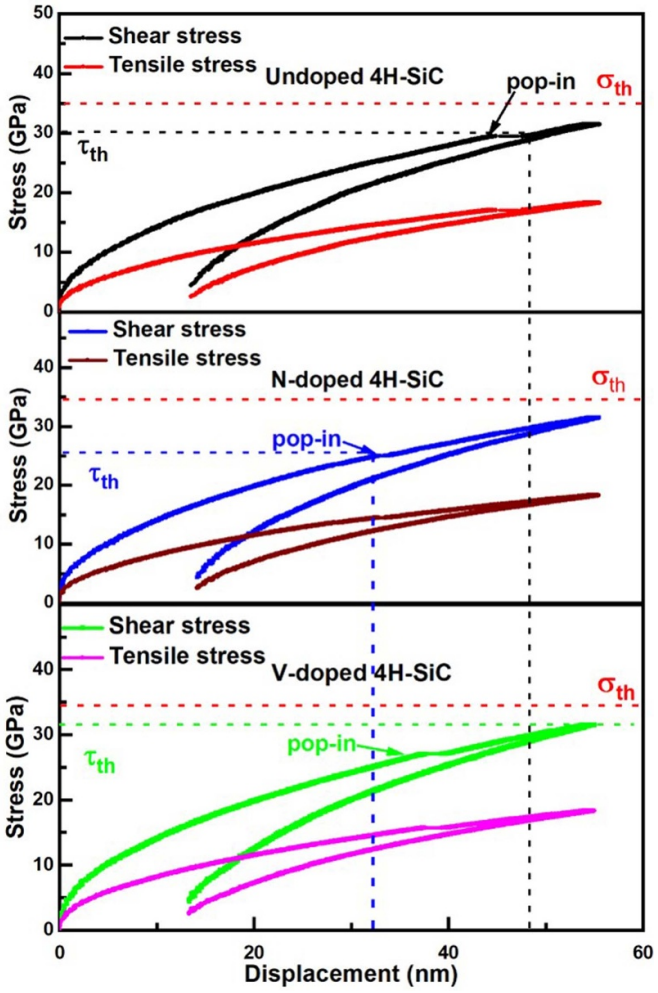

Figure 2. Calculated shear stress and tensile stress beneath the indenter as functions of the penetration depth in nanoindentated (a) undoped 4H-SiC, (b) N-doped 4H-SiC and (c) V-doped 4H-SiC. The theoretical shear strengths (τ_{th}) and theoretical cleavage strengths (σ_{th}) for the three samples are also enclosed as straight lines for comparison.

Table 1. The maximum shear stress (τ_{max}) and maximum tensile stress (σ_{max}) at the pop-in depth of undoped, N-doped and V-doped 4H-SiC. The theoretical shear strength (τ_{th}) and theoretical cleavage strength (σ_{th}) are also tabulated for comparison.

	τ_{max} (GPa)	τ_{th} (GPa)	σ_{max} (GPa)	σ_{th} (GPa)
Undoped 4H-SiC	29.45	29.76	17.10	33.00
N-doped 4H-SiC	25.35	25.5	14.57	33.00
V-doped 4H-SiC	27.05	31.47	15.66	33.00

The theoretical cleavage strength (σ_{th}) of 4H-SiC is calculated by Orowan's expression [26]: $\sigma_{th} = \frac{1}{2}\sqrt{\frac{E\gamma}{a}}$, where γ and a are the surface tension (36 J m^{-2}) [13], and interplanar spacing (2.53 Å) of 4H-SiC, respectively. As shown in figures 2(a)–(c) and table 1, the calculated tensile stresses during the whole loading–unloading cycle are always lower than the theoretical cleavage strength of 4H-SiC, regardless of the doping of 4H-SiC. This indicates that the formation of micro cracks does not occur for the low-load nanoindentated 4H-SiC. We note that the nanoindentation induced shear stress is much larger than the tensile stress for the three samples, indicating the deformation of 4H-SiC mainly originates from the shear stress [27].

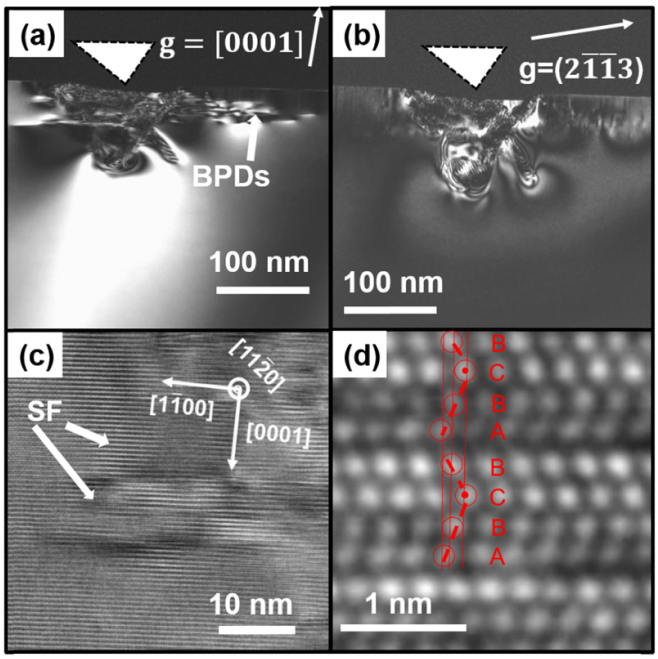

Figure 3. (a) The weak-beam dark-field TEM images of the undoped 4H-SiC at the pop-in depth using $g_1 = [0001]$ and (b) $g_2 = [2\bar{1}\bar{1}3]$. The indenter is indicated by the white triangle. (c) Cross-sectional HRTEM showing the basal-plane stacking faults (SFs) in the substrate taken at the $[11\bar{2}0]$ zone axis. (d) HRTEM image of undoped 4H-SiC taken from the region close to the nanoindentated region. The stacking sequence of basal atomic layers are guided by red lines.

Up to now, we find that dislocation nucleation is involved in the pop-in events of both undoped and N-doped 4H-SiC, while neither dislocation nucleation nor micro cracks gives rise to the pop-in event of V-doped 4H-SiC. Taking undoped and V-doped 4H-SiC as examples, we carry out TEM observations to clarify the detailed structural changes. As presented in figure 3(a), high density of dislocations is formed at the subsurface of nanoindentated 4H-SiC.

The Burgers vector of the dislocations are determined by the standard $g \cdot b = 0$ invisibility criterion, where g and b are diffraction reflection and Burgers vector, respectively. The same region under the indent is observed by the weak-beam dark filed TEM. It is clear that nanoindentation induced dislocations are in contrast with reflection $g_1 = [0001]$ and are out of contrast with $g_2 = [2\bar{1}\bar{1}3]$ (figures 3(a) and (b)). With the $g \cdot b = 0$ invisibility criterion, the Burgers vector of the nanoindentation induced dislocations is $\frac{1}{3}[01\bar{1}0]$. Furthermore, cross-sectional HRTEM images taken at the $[11\bar{2}0]$ zone axis clearly displays high density of stacking faults (SFs) bounded by partial dislocations (figure 3(c)). It is well known that the BPDs in 4H-SiC is prone to dissociate into partial dislocations separated by SFs according to the reaction: $\frac{a}{3}[11\bar{2}0] \rightarrow \frac{a}{3}[10\bar{1}0] + \frac{a}{3}[01\bar{1}0]$ [28]. Therefore, we attribute the low-load induced

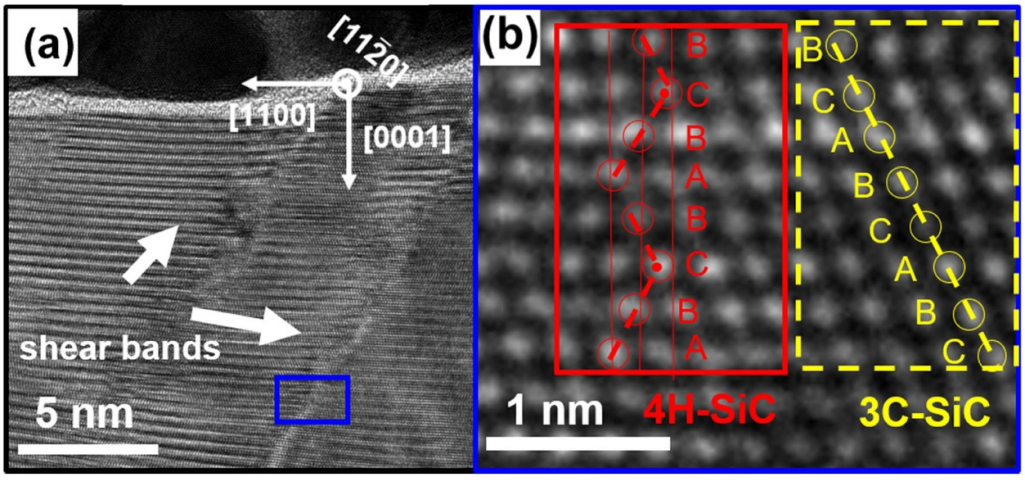

Figure 4. (a) HRTEM image of V-doped 4H-SiC at the pop-in depth taken from the region close to the indented region. (b) HRTEM image near the shear band showing the typical polymorph transition from 4H-SiC to 3C-SiC.

dislocations of undoped and N-doped 4H-SiC to BPDs. That is to say, the low-load nanoindentateation of undoped and N-doped 4H-SiC gives rise to he nucleation of BPDs. Figure 3(d) presents the HRTEM image of undoped 4H-SiC taken from the region close to the nanoindentated surface. It is clear that the atomic planes stacked in the sequence of ABCB, indicating polymorph transition does not occur during the nanoindentation, which agrees well with the theoretical stress filed calculations.

In order to clarify the structural changes in nanoindentated V-doped 4H-SiC, HRTEM observations on the region close to the nanoindentated region of V-doped 4H-SiC at the pop-in depth are then carried out. As shown in figure 4(a), micro cracks are not observed in the nanoindentated V-doped 4H-SiC, similar to what happens in undoped and N-doped samples. Two shear bands are found beneath the indenter surface. The zoom in image near the shear bands is shown in figure 4(b). The stacking sequence of ABC is observed near the shear bands, indicating partially polymorph transition from 4H-SiC to 3C-SiC is observed for V-doped 4H-SiC subjected to low loads.

At last, we discuss the role of doping on the nucleation of BPDs in 4H-SiC. For undoped 4H-SiC, the pop-in event corresponding to the elastic–plastic transition occurs at the displacement of 47 nm. Both theoretical calculations and TEM observations indicate that the initial plastic deformation is associated with the nucleation of BPDs. For N-doped 4H-SiC, the BPD-nucleation related pop-in event occurs at the displacement of 33 nm. This means that N doping facilitates the nucleation of BPDs in 4H-SiC. It is believed that the elastic strain may distort the conduction bands, which enhances the degeneracy of the conduction band edge and results in the redistribution of free carriers [29–31]. In N-doped 4H-SiC with high concentration of free electrons, the free-electron redistribution under the elastic strain is more prominent than that in semi-insulating undoped 4H-SiC. The enhanced free-electron redistribution reduces the free energy of N-doped 4H-SiC, and facilitates the nucleation of BPDs. For V-doped 4H-SiC, the first pop-in event corresponding to the polymorph transformation from 4H-SiC to 3C-SiC. Moreover, the polymorph transition occurs before the elastic–plastic transition. For 4H-SiC, the initial shear stress can be released by two ways either phase transition or dislocation nucleation induced by elastic–plastic transformation. In undoped and N-doped 4H-SiC, the shear stress is primary released through dislocation nucleation. While in V-doped 4H-SiC, the shear stress is released preferentially through polymorph transition rather than dislocation nucleation. During V doping, V atoms would replace Si atoms and forms V–C bonds in 4H-SiC [32]. Because the bonding strength of Si–C is smaller than that of V–C, the strength is enhanced in V-doped 4H-SiC, which hinders the nucleation of BPDs [33]. Therefore, the shear stress is released preferentially through phase transition rather than dislocation.

4. Conclusion

In conclusion, we have investigated the nucleation of BPDs, as well as the effect of doping on the BPD nucleation in 4H-SiC combining nanoindentation tests and TEM observations. We find that the shear stress prevails over the tensile stress in the low-load nanoindentation-induced stress field, which gives rise to the nucleation of BPDs in undoped 4H-SiC. N doping facilitates the BPD nucleation and decreases the shear stress required for the nucleation of BPDs. In contrast, V doping hinders the nucleation of BPDs, which promotes the polymorph transition from 4H-SiC to 3C-SiC. Our work completes the understanding on the nucleation of BPDs, and paves the way for the growth optimization and processing design of differently doped 4H-SiC wafers by reducing the density of BPDs.

Data availability statement

The data generated and/or analyzed during the current study are not publicly available for legal/ethical reasons but are available from the corresponding author on reasonable request.

Acknowledgments

This work is supported by 'Pioneer' and 'Leading Goose' R&D Program of Zhejiang (Grant No. 2022C01021), National Key Research and Development Program of China (Grant No. 2018YFB2200101), Natural Science Foundation of China (Grant Nos. 91964107 and 61774133), Fundamental Research Funds for the Central Universities (Grant No. 2018XZZX003-02), Natural Science Foundation of China for Innovative Research Groups (Grant No. 61721005) and Zhejiang University Education Foundation Global Partnership Fund.

Conflict of interest

The authors declare no conflict of interest.

ORCID iDs

Rong Wang https://orcid.org/0000-0003-3333-0180
Xiaodong Pi https://orcid.org/0000-0002-4233-6181

References

[1] Kimoto T and Cooper J A 2014 *Fundamentals of Silicon Carbide Technology: Growth, Characterization, Devices and Applications* (Singapore: John Wiley & Sons Singapore Pte. Ltd.)
[2] Casady J B and Johnson R W 1996 Status of silicon carbide (SiC) as a wide-bandgap semiconductor for high-temperature applications: a review *Solid-State Electron.* **39** 1409
[3] Yang S, Nakagawa Y, Kondo M and Shibayama T 2021 Anisotropic defect distribution in He^{+}-irradiated 4H-SiC: effect of stress on defect distribution *Acta Mater.* **211** 116845
[4] Shiramomo T, Gao B, Mercier F, Nishizawa S, Nakano S and Kakimoto K 2014 Study of the effect of doped impurities on polytype stability during PVT growth of SiC using 2D nucleation theory *J. Cryst. Growth* **385** 95
[5] Bing G and Koichi K 2014 Three-dimensional modeling of basal plane dislocations in 4H-SiC single crystals grown by the physical vapor transport method *Cryst. Growth Des.* **14** 1272
[6] He Y, Yuan Z, Song S, Gao X and Deng W 2021 Investigation on material removal mechanisms in photocatalysis-assisted chemical mechanical polishing of 4H-SiC wafers *Int. J. Precis. Eng. Manuf.* **22** 951
[7] Lukin D M *et al* 2020 4H-silicon-carbide-on-insulator for integrated quantum and nonlinear photonics *Nat. Photon.* **14** 330–4
[8] Tian Z, Xu X, Jiang F, Lu J, Luo Q and Lin J 2019 Study on nanomechanical properties of 4H-SiC and 6H-SiC by molecular dynamics simulations *Ceram. Int.* **45** 21998
[9] Nakashima S-I, Mitani T, Tomobe M, Kato T and Okumura H 2016 Raman characterization of damaged layers of 4H-SiC induced by scratching *AIP Adv.* **6** 015207
[10] Wang C, Zhang Y and Zhang Y 2007 Electrical and optical characteristics of vanadium in 4H-SiC *Chin. Phys.* B **16** 1417
[11] Cui Y, Hu X, Yang K, Yang X, Xie X, Xiao L and Xu X 2015 Influence of nitrogen concentrations on the lattice constants and resistivities of n-type 4H-SiC single crystals *Cryst. Growth Des.* **15** 3131
[12] Zhu B, Zhao D, Tian Y, Wang S, Zhao H and Zhang J 2019 Study on the deformation mechanism of spherical diamond indenter and its influence on 3C-SiC sample during nanoindentation process via molecular dynamics simulation *Mater. Sci. Semicond. Process.* **90** 143
[13] Nawaz A, Mao W G, Lu C and Shen Y G 2017 Nano-scale elastic-plastic properties and indentation-induced deformation of single crystal 4H-SiC *J. Mech. Behav. Biomed. Mater.* **66** 172
[14] Oliver W C and Pharr G M 1992 An improved technique for determining hardness and elastic modulus using load and displacement sensing indentation experiments *J. Mater. Res.* **7** 1564
[15] Liu X S, Zhang J R, Xu B J, Lu Y H, Zhang Y Q, Wang R, Yang D R and Pi X D 2022 Deformation of 4H-SiC: the role of dopants *Appl. Phys. Lett.* **120** 052105
[16] Oliver W C and Pharr G M 2004 Measurement of hardness and elastic modulus by instrumented indentation: advances in understanding and refinements to methodology *J. Mater. Res.* **19** 3
[17] Wu Z, Liu W and Zhang L 2020 Amorphization and dislocation evolution mechanisms of single crystalline 6H-SiC *Acta Mater.* **182** 60
[18] Zhao X, Langford R M, Shapiro I P and Ping X 2011 Onset plastic deformation and cracking behavior of silicon carbide under contact load at room temperature *J. Am. Ceram. Soc.* **94** 3509
[19] Matsumoto M, Huang H, Harada H, Kakimoto K and Yan J 2017 On the phase transformation of single-crystal 4H-SiC during nanoindentation *J. Phys. D: Appl. Phys.* **50** 265303
[20] Saurav G, Jiwang Y, Xichun L and Anupam A 2014 Incipient plasticity in 4H-SiC during quasistatic nanoindentation *J. Mech. Behav. Biomed. Mater.* **34** 330
[21] Hertz H 1882 On the contact elastic solids *J. Reine Angew. Math.* **92** 156
[22] Luo X, Goel S and Reuben R L 2012 A quantitative assessment of nanometric machinability of major polytypes of single crystal silicon carbide *J. Eur. Ceram.* **32** 3423
[23] Mao W and Shen Y 2012 Nanoindentation study of pop-in phenomenon characteristics and mechanical properties of sapphire ($10\bar{1}2$) crystal *J. Am. Ceram. Soc.* **95** 3605
[24] Gouldstone A, Koh H J, Zeng K Y, Giannakopoulos A E and Suresh S 2000 Discrete and continuous deformation during nanoindentation of thin films *Acta Mater.* **48** 2277
[25] Fischer-Cripps A C 2000 *Introduction to Contact Mechanics* (New York: Springer-Verlag New York, Inc.) (https://doi.org/10.1115/1.1470678)
[26] Veld A J G and Veldkamp J D E 1970 Mechanical and microscopical investigation of SiC whiskers *J. Fiber Sci. Technol.* **2** 269–81
[27] Zhu B, Zhao D and Zhao H 2019 Mechanical and microscopical investigation of SiC whiskers *Ceram. Int.* **45** 5150
[28] Chung S, Wheeler V, Ward R M, Eddy C R, Gaskill J D, Wu P, Picard Y N and Skowronski M 2011 A study of deformation behavior and phase transformation in 4H-SiC during nanoindentation process via molecular dynamics simulation *J. Appl. Phys.* **109** 094906
[29] Zeng Z, Ma X, Chen J, Zeng Y, Yang D and Liu Y 2010 Effects of heavy phosphorus-doping on mechanical properties of Czochralski silicon *J. Appl. Phys.* **107** 123503

[30] Latha H, Udayakumar A and Prasad V S 2014 The effect of nitrogen doping on the elastic modulus and hardness of 3C-SiC thin films deposited using methyltrichlorosilane *Mater. Res. Express* **1** 015902
[31] Keyes R W 1968 Electronic effects in the elastic properties of semiconductors *Solid State Phys.* **20** 37
[32] Mitchel W C, Perrin R, Goldstein J, Saxler A, Roth M, Smith S R, Solomon J S and Evwaraye A 1999 Fermi level control and deep levels in semi-insulating 4H–SiC *J. Appl. Phys.* **86** 5040
[33] Weast R C 1988 *CRC Handbook of Chemistry and Physics* (Boca Raton, FL: CRC Inc)